Reduced Encoding Diffusion Spectrum Imaging Implemented With a Bi-Gaussian Model

Chun-Hung Yeh, Kuan-Hung Cho, Hsuan-Cheng Lin, Jiun-Jie Wang, and Ching-Po Lin*

***Abstract*—Diffusion spectrum imaging (DSI) can map complex fiber microstructures in tissues by characterizing their 3-D water diffusion spectra. However, a long acquisition time is required for adequate q-space sampling to completely reconstruct the 3-D diffusion probability density function. Furthermore, to achieve a high q-value encoding for sufficient spatial resolution, the diffusion gradient duration and the diffusion time are usually lengthened on a clinical scanner, resulting in a long echo time and low signal-to-noise ratio of diffusion-weighted images. To bypass long acquisition times and strict gradient requirements, the reduced-encoding DSI (RE-DSI) with a bi-Gaussian diffusion model is presented in this study. The bi-Gaussian extrapolation kernel, based on the assumption of the bi-Gaussian diffusion signal curve across biological tissue, is applied to the reduced q-space sampling data in order to fulfill the high q-value requirement. The crossing phantom model and the manganese-enhanced rat model served as standards for accuracy assessment in RE-DSI. The errors of RE-DSI in estimating fiber orientations were close to the noise limit. Meanwhile, evidence from a human study demonstrated that RE-DSI significantly decreased the acquisition time required to resolve complex fiber orientations. The presented method facilitates the application of DSI analysis on a clinical magnetic resonance imaging system.**

***Index Terms*—Bi-Gaussian model, diffusion spectrum imaging, manganese-enhanced rat model, phantom model.**

I. Introduction

DIFFUSION magnetic resonance imaging (MRI) has become an essential tool for contrast imaging of the central nervous system and led to significant improvement in clinical diagnosis. Further advancement to the technique has been made with the introduction of diffusion tensor imaging (DTI) [1], [2], a valuable technique in characterizing anisotropic diffusion as well as noninvasively delineating the principle orientations of white matter tracts [3]–[5]. However, the assumption of a single Gaussian diffusion compartment in the tensor model results in the ambiguous orientation of neural fibers in regions where they cross each other. [6]. Thus, with the typical imaging resolution of an MRI scanner, it may be difficult to interpret the complex neural connections between functional areas of the human brain due to the partial volume effect.

In recent years, various diffusion MR imaging strategies have been developed to improve the interpretation of diffusion function and to resolve the intravoxel fiber orientations. Diffusion spectrum imaging (DSI) [7] utilizes the 3-D spectra of water displacement to characterize the heterogeneity of fiber architecture. The principle of DSI is established on the theory of the q-space imaging technique. The theory describes the Fourier relationship between echo signal attenuation and the probability density function (PDF) of the displacement of water molecules with the prerequisite of a narrow pulse approximation [8]–[10]. DSI has been used to map the tissue architecture of biological systems [7], [11]. Specifically, it provides the intravoxel compartment scales of neural fibers [12], thus allowing physiological and structural conditions of neural tissues to be interpreted. Furthermore, 3-D tractography and comparative segmentation of human brain structures have also been identified based on the DSI technique [13].

Nevertheless, a complete reconstruction of the diffusion PDF in DSI requires an exhaustive q-space sampling of 515 q-value encoding points distributed on a Cartesian lattice across 3-D q-space. This involves long acquisition times as well as adequate q-values for sufficient resolution. Since the available gradient strength in the clinical system is limited, the latter requirement is achieved by prolonging the diffusion gradient duration (δ) and the diffusion time (Δ); thus resulting in a long echo time (TE) and a decline in the signal-to-noise ratio (SNR) due to a severe T2 decay in the echo planar imaging (EPI) sequence. In consequence, angular accuracy and discrimination are inevitably diminished [11]. The lengthy acquisition times and the requirements of the gradient system have hindered the further application of DSI on clinical scanners.

A hemispheric encoding scheme (half-q-DSI) can be applied to halve the scan time in DSI since the diffusion contrast is positive and spherically symmetric [7], [14]. However, the uncorrected cross-term interactions between diffusion and imaging gradients might result in the misinterpretation of the q-space analysis and inaccurate orientation distribution function (ODFs) in half-q-DSI [15], [16]. In addition, a body-center-cubic (BCC) sampling scheme was proposed instead of a Cartesian lattice to improve the imaging efficiency of DSI by 30% [17]. Hybrid diffusion imaging (HYDI) employs another non-Cartesian q-space encoding scheme for DSI-PDF reconstruction [18]. This scheme

Manuscript received September 30, 2007; revised February 18, 2008. First published July 22, 2008; current version published September 24, 2008. This work was supported by the National Science Council of Taiwan under Grant 97-2752-H-010-004-PAE. *Asterisk indicates corresponding author.*

C.-H. Yeh and H.-C. Lin are with the Department of Biomedical Imaging and Radiological Sciences, National Yang-Ming University, Taipei, Taiwan.

K.-H. Cho is with the Interdisciplinary MRI/MRS Laboratory, Department of Electrical Engineering, National Taiwan University, Taipei, Taiwan.

J.-J. Wang is with the Institute of Medical Physics and Imaging Science, Chang Gung University, Taoyuan, Taiwan.

*C.-P. Lin is with the Department of Biomedical Imaging and Radiological Sciences, National Yang-Ming University, Taipei, Taiwan, and with the Laboratory for Brain Connectivity, Institute of Neuroscience, National Yang-Ming University, Taipei, Taiwan and also with the Institute of Brain Science, National Yang-Ming University, Taipei, Taiwan, (e-mail: cplin@ym.edu.tw).

Color versions of one or more of the figures in this paper are available online at http://ieeexplore.ieee.org.

Digital Object Identifier 10.1109/TMI.2008.922189

comprises five concentric spherical shells and can be applied to multiple types of diffusion analysis. Although it is possible to shorten the scan times with the q-space sampling strategies described above, the requirement of high q-space acquisitions could not be omitted to preserve adequate spatial resolution.

Another category of diffusion imaging techniques utilizes an encoding scheme formed by a single spherical shell with a constant diffusion weighting as opposed to the 3-D Cartesian lattice with multiple diffusion weightings. These techniques include high angular resolution diffusion imaging (HARDI) [19], [20], q-ball imaging (QBI) [21], [22], persistent angular structure MRI (PAS-MRI) [23], fiber orientation estimated using continuous axially symmetric tensors (FORECAST) [24], diffusion orientation transform (DOT) [25], and spherical deconvolution methods [26], [27]. These approaches provide information on the orientation of complex neural fiber networks within a reasonable scan time and can be routinely implemented. The substantial increase in imaging efficiency mainly results from the fewer number of diffusion-weighted images (DWIs) required for data analysis. Meanwhile, the moderate b-value followed by a shortened TE can enhance the SNR of DWIs. These techniques however, may be insufficient to characterize the 3-D diffusion function that can be derived from multiple q-value diffusion measurements, and would thus be unable to infer microstructural conditions in tissues.

In this study, the reduced-encoding DSI complemented with a bi-Gaussian model (RE-DSI) is proposed in order to trim down the drawbacks of DSI while retaining q-space information. In RE-DSI, a reduced Cartesian sampling scheme, where the acquisitions at high q-space are omitted, is used to bypass long acquisition times and gradient system demands in DSI. To achieve sufficient resolution for fiber orientation estimation, the 1-D bi-Gaussian model is applied to the sampled data at low q-space to regain all diffusion signals at high q-space. Previous studies on animal and human brains have demonstrated that diffusion-attenuated curves can be characterized as a bi-exponential function [28]–[31]. Accordingly, we hypothesize that the diffusion signal attenuation along each radial direction in q-space would follow a bi-Gaussian function. This assumption is similar to that used in the DOT technique [25] which directly converts the diffusivity function into displacement probabilities at a particular distance away from the origin, while RE-DSI tends to reconstruct a whole diffusion PDF from q-space signals.

The performance of RE-DSI in terms of accurately defining the orientations of both coherent and heterogeneous fibers was assessed using the capillary phantom model and the manganese-enhanced (ME) rat model. These models have been previously utilized to validate the DTI and DSI techniques [5], [11]. The magnetic resonance (MR) images of capillary phantoms and the ME rat optic tract served as the standard for the measurement of angular uncertainties in RE-DSI. The results show that the resulting PDF profiles and ODF patterns reconstructed by RE-DSI were comparable to those achieved by DSI. The merits of RE-DSI in a clinical environment are twofold: 1) the scan time can be remarkably shortened to a half or a quarter of its original time and 2) shorter TE allows for the acquisition of DWIs with relatively high SNR under limited gradient intensity. To demonstrate the clinical feasibility of RE-DSI, this technique was applied to a healthy subject at the end of this study.

II. Materials and Methods

A. Reduced-Encoding Scheme

In DSI, the q-space sampling scheme consists of 515 diffusion wave vectors q, where $q = \gamma g \delta / 2\pi$ (γ: gyromagnetic ratio; g: gradient vector; δ: duration of diffusion gradient), placed on a Cartesian lattice within a sphere that has a radius of five lattice units [7]. The framework of the q-space acquisition scheme in RE-DSI is the same as that of DSI, except the encoding wave vectors are within a radius of three or four lattice units, giving the encoding numbers of 123 and 257, respectively.

B. Bi-Gaussian Model

Assumption of the bi-Gaussian model in RE-DSI was established according to several studies on bi-exponential analyses of high b-value diffusion data [28]–[31]. The bi-exponential diffusion signal decay model, also called the two-compartment model, ascribes the contribution of MR signal attenuation to the weighted sum of fast and slow water diffusion. The general formula is shown as follows [32]:

$$\frac{S(b)}{S_0} = f_{\text{slow}} \exp(-bD_{\text{slow}}) + f_{\text{fast}} \exp(-bD_{\text{fast}}) \quad (1)$$

where b is the diffusion-sensitizing factor defined as $b = (\gamma g \delta)^2 \Delta$ or $b = 4\pi^2 q^2 \Delta$, $S(b)$ is diffusion signal associated with the b-value and S_0 is the signal value without diffusion weighting ($b = 0$), f_{slow} and f_{fast} represents the fraction of slow diffusion (D_{slow}) and fast diffusion (D_{fast}) compartment, respectively. From (1), the bi-Gaussian model can be formed with the echo signal expressed as a function of the q-value, i.e.,

$$\frac{S(q)}{S_0} = f_{\text{slow}} \exp(-4\pi^2 q^2 \Delta D_{\text{slow}}) + f_{\text{fast}} \exp(-4\pi^2 q^2 \Delta D_{\text{fast}}) \quad (2)$$

where f_{slow}, f_{fast}, D_{slow}, and D_{fast} are the parameters to be optimized during curve fitting. By fitting the reduced-encoding diffusion data with (2), signal values at specific q-values can be estimated from the fitted curves. The detailed procedures are summarized as follows.

1) Selecting a target gradient vector q that determines the 1-D radial direction passing through the origin and the target.
2) Performing the spherical radial basis function (sRBF) interpolation [21] on undersampled data to generate diffusion signals along the chosen 1-D radial direction in q-space.
3) Fitting the interpolated signals with the bi-Gaussian model (2) using the nonlinear least squares fitting method. Model coefficients were optimized using the trust region algorithm [33] implemented with the curve fitting toolbox of MATLAB (The MathWorks).
4) After retrieving signal values at high q space from the fitted curve, return to 1) and repeat until all of the (515) q-space signals are recovered.

C. Phantom Study

Numerous plastic capillaries with an inner diameter of 20 μm and outer diameter of 90 μm (Polymicro Technologies, Phoenix, AZ) were compactly arranged in a parallel direction. Two bundles of capillaries were stacked onto each other to simulate two fibers crossing: one intersecting at 45° and the other at 90°. The design of capillary phantoms allowed for an ideal restrictive environment that was analogous to the scale of diffusion measurement.

Crossing phantoms were scanned with a Bruker 9.4-T Biospec MRI system equipped with a micro-gradient system and had a maximum gradient strength of 1463 mT/m. T2-weighted images (T2WIs) were acquired using the rapid acquisition with relaxation enhancement sequence (RARE), where TR/TE $=$ 2500/4.4 ms, matrix size $=$ 256 $\times$ 256 and voxel dimension $=$ 0.078 $\times$ 0.078 $\times$ 3.2 mm^3. For each phantom, five DSI datasets with the all 515 sampling points were acquired by the stimulated echo pulsed gradient sequence using the following parameters: matrix size $=$ 32 $\times$ 32, voxel dimension $=$ 0.75 $\times$ 0.75 $\times$ 3.2 mm^3, TR/TE $=$ 1,000/17.8 ms, Δ/δ $=$ 200/5 ms. Diffusion gradients were altered from 0 to 184 mT/m, yielding a maximum q-value ($q_{\max}$) and a maximum b-value ($b_{\max}$) of 39.1 mm^{-1} and 12 000 s/mm^2 respectively. The acquisition time for each DSI dataset was approximately 10 h, and the total scan time for each phantom was around 50 h. For comparison, the reconstruction of RE-DSI was applied to the signals at a low q-space of the DSI dataset in this study. The cutoff q-values were 31.3 and 23.5 mm^{-1} for RE-DSI-257 and RE-DSI-123, respectively.

D. Manganese-Enhanced Rat Study

The ME rat model provided a standard for the accuracy assessment of diffusion MR techniques in mapping neural fiber directions [5], [11]. Animal preparation procedures were in accordance with the Guidelines for Care and Use of Experimental Animals of the Laboratory Animal Center in National Taiwan University. Adult Wistar rats were first anesthetized with an intraperitoneal injection of sodium pentobarbital at a dose of 0.05 mg per gram of body weight. Then, 2 μL of manganese chloride solution at a concentration of 0.8 mol/L was infused into the vitreal cavity of the rats' eyes using a micropipette needle. Ten hours after infusion, the rats were euthanized under deep general anesthesia using an intraperitoneal injection of 100 mg/kg sodium pentobarbital. They were then placed into a prone position in an acrylic semicylindrical holder with their heads fixed by foam pads. The holder was then inserted into an animal gradient system for scanning.

MR experiments on ME rats were performed using a Bruker 3-T Medspec/Biospec MRI system installed with a gradient system of maximum gradient strength equal to 200 mT/m. Sagittal T1-weighted images (T1WIs) were first obtained as reference scans from which two oblique slices containing ME fiber tracts were determined [5]. One contained optic tracts from the bilateral retina to the optic chiasm, and the other covered the area from the optic chiasm to the superior colliculus (SC). The same field-of-view (FOV) of 40 mm and slice thickness of 1.2 mm were set for both T1WI and DSI. T1WIs were acquired using an inversion recovery gradient echo sequence with the following imaging parameters: flip angle $=$ 75°, TR/TE/TI $=$ 505/5.1/320 ms, matrix size $=$ 256 $\times$ 256, and yielding in plane resolution $=$ 0.16 $\times$ 0.16 mm^2. Complete q-space sampling of DSI datasets were obtained using a spin echo pulsed gradient sequence with matrix size $=$ 128 $\times$ 128, yielding in plane resolution $=$ 0.31 $\times$ 0.31 mm^2, TR/TE $=$ 2000/51.5 ms, and Δ/δ $=$ 25/17 ms. Diffusion gradients were increased from 0 to 158 mT/m, yielding a $q_{\max}$ $=$ 114.5 mm^{-1} and a $b_{\max}$ $=$ 10 000 s/mm^2. The DSI experimental time was approximately 36 h, and the reconstruction of RE-DSI was also applied to the signals at a low q-space of the DSI dataset using the cutoff q-values of 91.6 and 68.7 mm^{-1} for RE-DSI-257 and RE-DSI-123, respectively.

E. Human Study

DSI and RE-DSI data of a single healthy subject were obtained using a 1.5-T GE SIGNA scanner (GE Healthcare) with a diffusion-weighted echo-planar imaging sequence. DSI data was acquired using a conventional q-space sampling scheme with 515 points. Acquisition of RE-DSI utilized the reduced-encoding schemes with 257 and 123 sampling points. Three oblique slices were obtained with matrix size $=$ 64 $\times$ 64 and voxel dimension $=$ 3.6 $\times$ 3.6 $\times$ 3.6 mm^3 under TR $=$ 3000 ms. Other imaging parameters were Δ $=$ 56.0, 49.0, and 41.4 ms; δ $=$ 47.8, 40.8, and 33.2 ms; $b_{\max}$ $=$ 10 000, 6400, and 3600 s/mm^2; $q_{\max}$ $=$ 79.5, 67.6, and 54.8 mm^{-1}; TE $=$ 139.2, 122.7, and 104.8 ms; scan times $=$ 26, 13, and 6 min for 515, 257, and 123 sampling points, respectively.

F. RE-DSI Reconstruction

Data analysis for RE-DSI is identical to that of DSI [7], [11]. The 3-D PDF of diffusion displacement is reconstructed using the Fourier transformation of the q-space signals [9], as indicated in

$$E_{\Delta}(q) = \int \mathrm{PDF}(R, \Delta) \exp(i2\pi q \cdot R) dR \tag{3}$$

where E_{Δ} is the normalized q-space signal measured at a diffusion time Δ, and R is the average displacement of water molecules. Angular structure of the 3-D PDF is then visualized through the ODF, which is defined as the radial integral of PDF over the radial dimension [7], [11]

$$\mathrm{ODF}(u) = \int_0^{r_{\max}} \mathrm{PDF}(ru) r^2 dr \tag{4}$$

where $r_{\max}$ the upper limit of the integration, is defined as the linear FOV of the PDF and is equal to the reciprocal of the minimum q-value ($q_{\min}$), i.e., $r_{\max} = q_{\min}^{-1}$. ODF measures the quantity of water molecules diffused along the unit vector u. Primary fiber orientations in each voxel were defined as the local maximum vectors of ODFs in this study.

G. Angular Uncertainties in RE-DSI

The omission of high q-value acquisition has a great impact on the angular discrimination and accuracy. To reduce the drawbacks that result from undersampling in q-space, high q-space

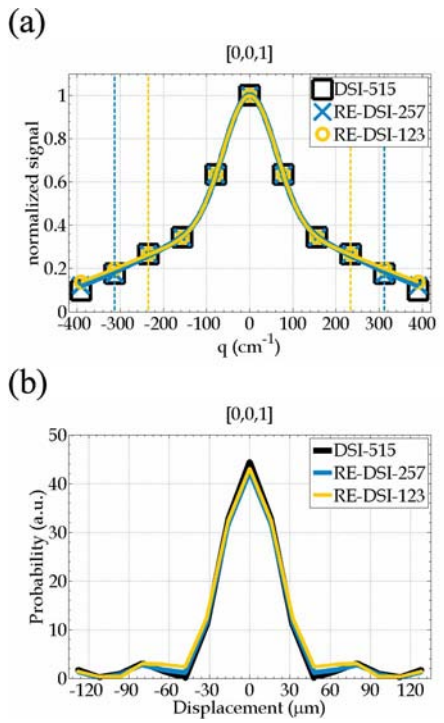

Fig. 1. The signal profiles, bi-Gaussian fitting curves, and the PDF profiles along the unit vector (0,0,1) of the 90° phantom model. (a) The vertical dashed lines colored in blue and orange denote the q-value cutoff of 31.3 and 23.5mm^{-1} for RE-DSI-257 and RE-DSI-123, respectively. The acquired MR signal values, i.e., DSI-515, are shown in black. Signal values for RE-DSI-257 and RE-DSI-123 with their respective bi-Gaussian fitting curves are colored in blue and orange. (b) Black, blue, and orange curves are the PDF profiles corresponding to the signal profiles of DSI-515, RE-DSI-257, and RE-DSI-123.

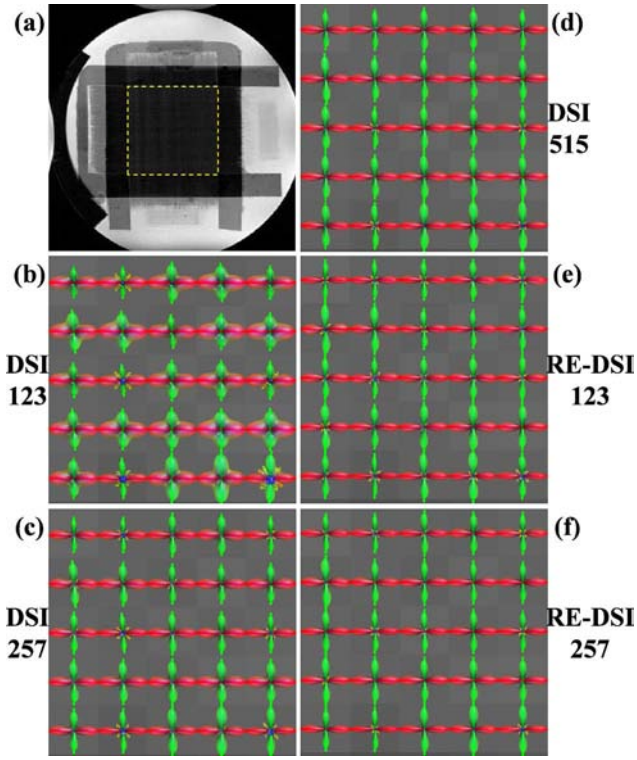

Fig. 2. The phantom in a 90° intersection between sheets served as a standard to evaluate DSI results with and without application of the bi-Gaussian extrapolation. (a) The angle between intersecting capillaries, measured on high resolution T2WI, was regarded as the standard. (b)–(d) ODFs obtained directly from DSI processing with encoding numbers 123, 257, and 515, respectively. The shapes of ODFs became improper as the q-encoding number decreased. (e)–(f) Shapes of ODFs were well preserved when the bi-Gaussian extrapolation kernel was applied to the reduced encoding points of 123 and 257.

signal values were regained in RE-DSI with implementation of the bi-Gaussian extrapolation kernel. For convenience sake, conventional DSI with 515 q-space sampling is abbreviated to DSI-515 in this study. Similarly, DSI directly reconstructed from the reduced-encoding data of 257 and 123 sampling are abbreviated to DSI-257 and DSI-123. These are different from RE-DSI-257 and RE-DSI-123.

The phantom models were designed to assess the effect of q-space encoding numbers on RE-DSI in regards to angular uncertainties. First, angular discrimination was compared between DSI-257, DSI-123, RE-DS-257, and RE-DSI-123 to verify the necessity of the bi-Gaussian extrapolation. Second, angular accuracy in DSI-515, RE-DSI-257, and RE-DSI-123 were compared according to the deviation angle and the success rate. Since reduced sampling schemes are generally more susceptible to background noise contamination [34], in order to equalize the amount of DWIs, i.e., the SNR level, two and four datasets were averaged for RE-DS-257 and RE-DSI-123 reconstructions respectively. Third, data averaging of five DSI datasets facilitated the measurement of uncertainties in RE-DSI under various SNR levels. SNR was measured on the nondiffusion-weighted ($b = 0$) image at a region of interest (ROI) containing crossing capillaries, as the dotted polygons show in Fig. 2(a) and Fig. 3(a). The SNRs were around 2.5, 3.5, 4.5, 5.0, and 5.6. In the phantom studies, 45° and 90° crossings measured from high resolution T2WIs [Fig. 2(a) and Fig. 3(a)] served as the standard for the accuracy assessment. The deviation angle was defined as the difference between the intersection angle of local maximum vectors and the standard. The success rate was defined as the percentage of identifying two distinct local maximum vectors from the ODFs in the ROI.

With contrast enhancement, optic tracts clearly visualized on T1WIs [Fig. 3(a) and Fig. 4(a)] were considered as the standard. To segment and visualize the optic tracts, a magnitude threshold was first applied to the ME T1WI, and the enhanced pixels were then fitted with a six-order polynomial function. The tangential vector at any location was determined from the derivative of the polynomials. The deviation angle in the rat studies was defined as the angle between the tangential vector of the ME optic tract and the local maximum vector [5], [11].

III. Results

A. Comparison Between DSI and RE-DSI

Fig. 1(a) is an illustration of the bi-Gaussian fitting curves on the reduced set of q-values from the 90° phantom and the comparison between the high q-space signals estimated from the fitting curves and those acquired in experiments, i.e., the signals of DSI-515. The signal profiles of RE-DSI-257 and RE-DSI-123 matched well with that of DSI-515. Fig. 1(b) shows the respective 1-D diffusion PDF derived from DSI and RE-DSI. The plot

TABLE I
DEVIATION ANGLES OF THE STANDARD DSI AND RE-DSI ON PHANTOM MODELS UNDER EQUAL SNR LEVELS

	DSI-515 (NEX = 1)		RE-DSI-257 (NEX = 2)		RE-DSI-123 (NEX = 4)	
Crossing phantom	Mean ± SD	Success	Mean ± SD	Success	Mean ± SD	Success
90°	0.03° ± 0.23°	100 %	0.04° ± 0.28°	100 %	0.03° ± 0.26°	100 %
45°	2.17° ± 0.65°	100 %	2.10° ± 0.20°	100 %	4.70° ± 3.51°	89 %

A hundred voxels were analyzed for both 90° and 45° crossing phantoms.

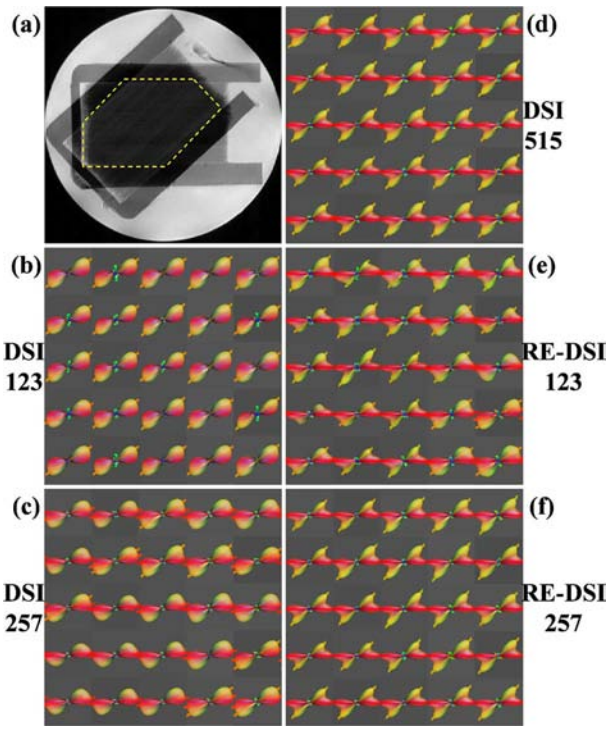

Fig. 3. The phantom in a 45° intersection between sheets. (a) T2WI of the 45° crossing phantom. (b)–(d) The ODFs of DSI with encoding numbers 123, 257, and 515, respectively. Ambiguous fiber orientations observed in Fig. 3(a) and (c) were caused by the reduction in angular sampling of DSI. Intersecting capillaries were successfully differentiated by RE-DSI of 123 (e) and 257 (f) sampling points.

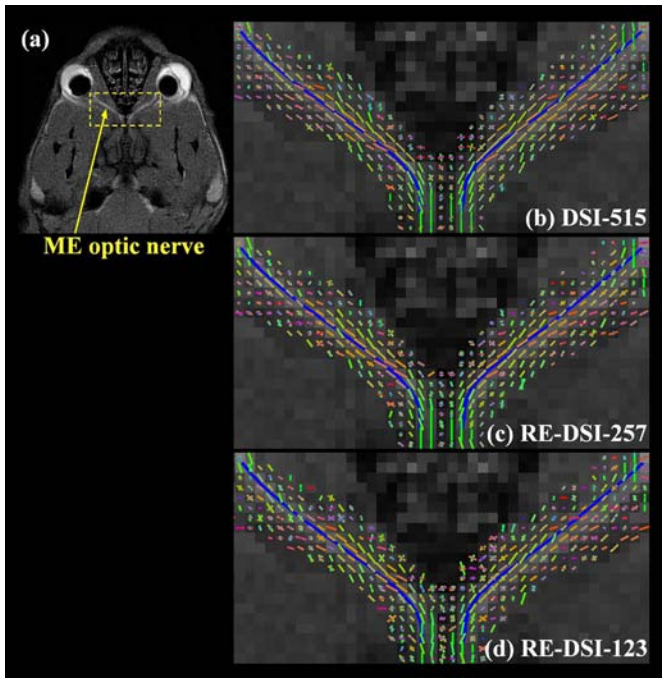

Fig. 4. T1WI of manganese-enhanced rat optic nerves served as a reference to evaluate the RE-DSI. (a) Manganese was injected into the retina to enhance rat optic tracts from the retina to the optic chiasm which can be clearly identified with T1WI. (b)–(d) Segmented via the threshold and curve fitting methods, the ME optic nerves (blue lines) were superimposed on the field of local maximum vectors of DSI and RE-DSI. The deviation angles between the ME optic nerves and the local maximum vectors were measured for each q-space encoding framework. The results show that RE-DSI is a promising method to delineate fiber orientation in biological tissue.

demonstrated that RE-DSI can feasibly preserve the PDF features and thus the ODF of DSI.

ODFs and local maximum vectors of phantom models calculated from DSI and RE-DSI are shown in Figs. 2 and 3. The angular uncertainties in defining 90° and 45° fiber crossings are summarized in Table I. T2WIs of 90° and 45° phantoms are shown in Fig. 2(a) and Fig. 3(a), where ROIs for quantifying angular uncertainties are highlighted in the dotted polygons. DSI-515 successfully mapped all voxels containing 90° [Fig. 2(d)] and 45° crossing capillaries [Fig. 3(d)] with errors of $0.03° \pm 0.23°$ and $2.17° \pm 0.65°$ (Table I), respectively. Both DSI-123 and DSI-257 were sufficient to differentiate a 90° intersecting angle [Fig. 2(b) and (c)] but failed in the 45° case [Fig. 3(b) and (c)]. Even if two directions were resolved, the intersection angle deviated from 45°. The results demonstrate that high q-value signals are crucial to angular discrimination. In contrast, RE-DSI succeeded in resolving both 90° and 45° crossing angles. The results of RE-DSI-257 are shown in Fig. 2(f) and Fig. 3(f). ODF features were properly preserved in comparison with those of DSI-515. The errors were $0.04° \pm 0.28°$ and $2.10° \pm 0.20°$ in the case of 90° and 45° crossings respectively. In RE-DSI-123, ODFs shown in Fig. 2(e) and Fig. 3(c) were also well preserved, although a few of them were not sharp enough to detect two fiber crossing at 45°. Additionally, undesired fictitious ODFs (UFO) may have emerged from errors originating from the bi-Gaussian fitting of undersampled data. The errors were $0.03° \pm 0.26°$ and $4.70° \pm 3.51°$ in the case of 90° and 45° crossing, respectively. The slightly increased error for the case of 45° crossing in RE-DSI-123 may have resulted from fewer q-space acquisitions.

B. Noise Tolerance of RE-DSI

Tolerance of RE-DSI to noise was assessed with the 45° phantom model. Quantitative results of angular deviations and success rates under various SNR levels are listed in Table II. Lower SNR levels caused greater angular errors and peaking of UFO in RE-DSI. In comparison with RE-DSI-123, RE-DSI-257 demonstrated a higher resistance to noise contamination. With RE-DSI-257, it was possible to resolve two distinct fiber directions intersecting at 45° with an error of $2.27° \pm 0.82°$ under

TABLE II
EVALUATION OF THE EFFECT OF NOISE ON RE-DSI WITH A 45° CROSSING PHANTOM

	RE-DSI-257		RE-DSI-123	
NEX (SNR)	Mean ± SD	Success	Mean ± SD	Success
5 (5.6)	2.14° ± 0.23°	100 %	4.70° ± 3.51°	90 %
4 (5.0)	2.12° ± 0.21°	100 %	5.21° ± 5.13°	89 %
3 (4.5)	2.13° ± 0.22°	100 %	5.31° ± 3.70°	86 %
2 (3.5)	2.10° ± 0.20°	100 %	7.48° ± 5.03°	72 %
1 (2.5)	2.27° ± 0.82°	100 %	7.57° ± 6.11°	74 %

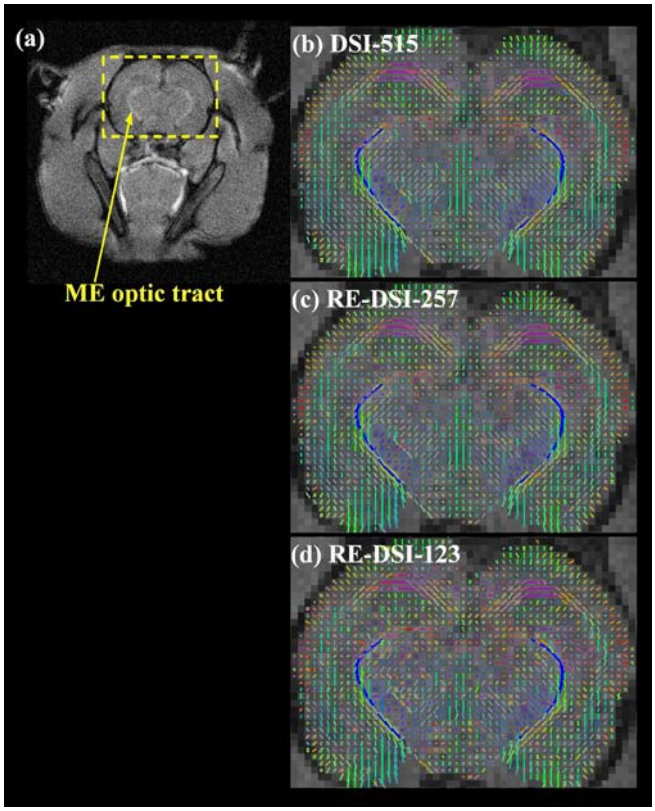

Fig. 5. (a) Manganese-enhanced T1WI of rat optic tracts. T1WI clearly showed the enhanced optic tract extending from the optic chiasm to the superior colliculus. (b)–(d) With the same image processing method, the segmented optic tracts (blue) were visualized and superimposed on the field of local maximum vectors.

a SNR level of 2.5. However, in RE-DSI-123, the success rate declined to around 70% at a SNR level of 3.5 with deviation angles of $7.48° \pm 5.03°$. These results suggest that the SNR limit for RE-DSI-123 was 3.5 in these phantom models.

C. ME Rat Model

The anatomical structures of ME optic nerves were visualized with the substantial enhancement of T1WIs. The T1WI in Fig. 4(a) clearly illustrates the ME optic nerve spanning from the retina to the optic chiasm. Fig. 4(b)–(d) shows maps of the local maximum vectors derived from DSI-515, RE-DSI-257 and RE-DS-123 superimposed on the ME T1WI with the segmented optic nerves colored in blue. In Fig. 5(a), the enhanced optic tracts extending from optic chiasm to SC are shown on the ME T1WI which was superimposed with the maps of local maximum vectors as shown in Fig. 5(b)–(d). Table III summarizes the errors in defining the directions of ME optic tracts for DSI-515, RE-DSI-257, and RE-DSI-123. Despite a slight increase in angular errors, the results of RE-DSI were close to those of DSI.

TABLE III
MEAN AND MAXIMUM ANGLE DEVIATIONS FOR THE MANGANESE-ENHANCED RAT MODEL FOR STANDARD DSI AND RE-DSI

	DSI-515	RE-DSI-257	RE-DSI-123
Rat model	Mean ± SD	Mean ± SD	Mean ± SD
Optic nerve	5.2° ± 6.1°	5.5° ± 5.8°	6.4° ± 6.9°
Optic tract	7.1° ± 5.5°	7.9° ± 6.6°	8.9° ± 9.0°

D. Human Brain Imaging

Fig. 6 illustrates the DSI and RE-DSI of a brain slice. The T1WI with the corresponding slice location is shown in Fig. 6(a) and the ODF map of the whole slice derived from DSI-515 is shown in Fig. 6(b). ODFs were color-coded according to their orientations; red, green, and blue indicated superior–inferior, medial–lateral, and anterior–posterior, respectively. Fig. 6(c)–(h) shows the zoomed areas of the centrum semiovale and brainstem for DSI-515, RE-DSI-257, and RE-DSI-123. Fig. 6(c), (e), and (g) show a clear intersection of the corpus callosum (green) and corticospinal tract (red), as highlighted by the blue dotted squares. DSI and RE-DSI succeeded in resolving crossing fibers at the centrum semiovale. In Fig. 6(d), (f), and (h), it can be seen that the orientations of the corticospinal tracts (red) and middle cerebellar peduncle (green) were well resolved by DSI and RE-DSI. With the exception of a few errors arising from RE-DSI-123 due to the effect of fewer q-space sampling, the results of RE-DSI were comparable to those of DSI. This is shown in the area marked by the white rectangle in Fig. 6(h).

IV. DISCUSSION

By extension from 1-D q-space imaging, DSI can depict a 3-D diffusion PDF through exhaustive sampling over 3-D q-space. Although DSI employs a suboptimal encoding scheme that might impede its practical applications, the invaluable information from multiple q-value measurements may be beneficial in interpreting the structural conditions of biological tissues. The current study indicates that RE-DSI makes it possible to bypass long acquisition times and strict gradient requirements while preserving the characteristics of DSI. The reduced-encoding scheme allows RE-DSI to improve imaging efficiency as well as to increase the SNR of DWIs under limited gradient intensity in a clinical system, while the bi-Gaussian model introduced in 1-D space can retrieve the angular resolution. We demonstrate the angular accuracy of RE-DSI by assessing with the crossing phantom model, and the capacity for fiber orientation estimation in a biological system is verified by the ME rat model. Furthermore, the result of a human brain study indicates that RE-DSI can feasibly resolve intersections of white matter within a reasonable scan time using a clinical MR scanner.

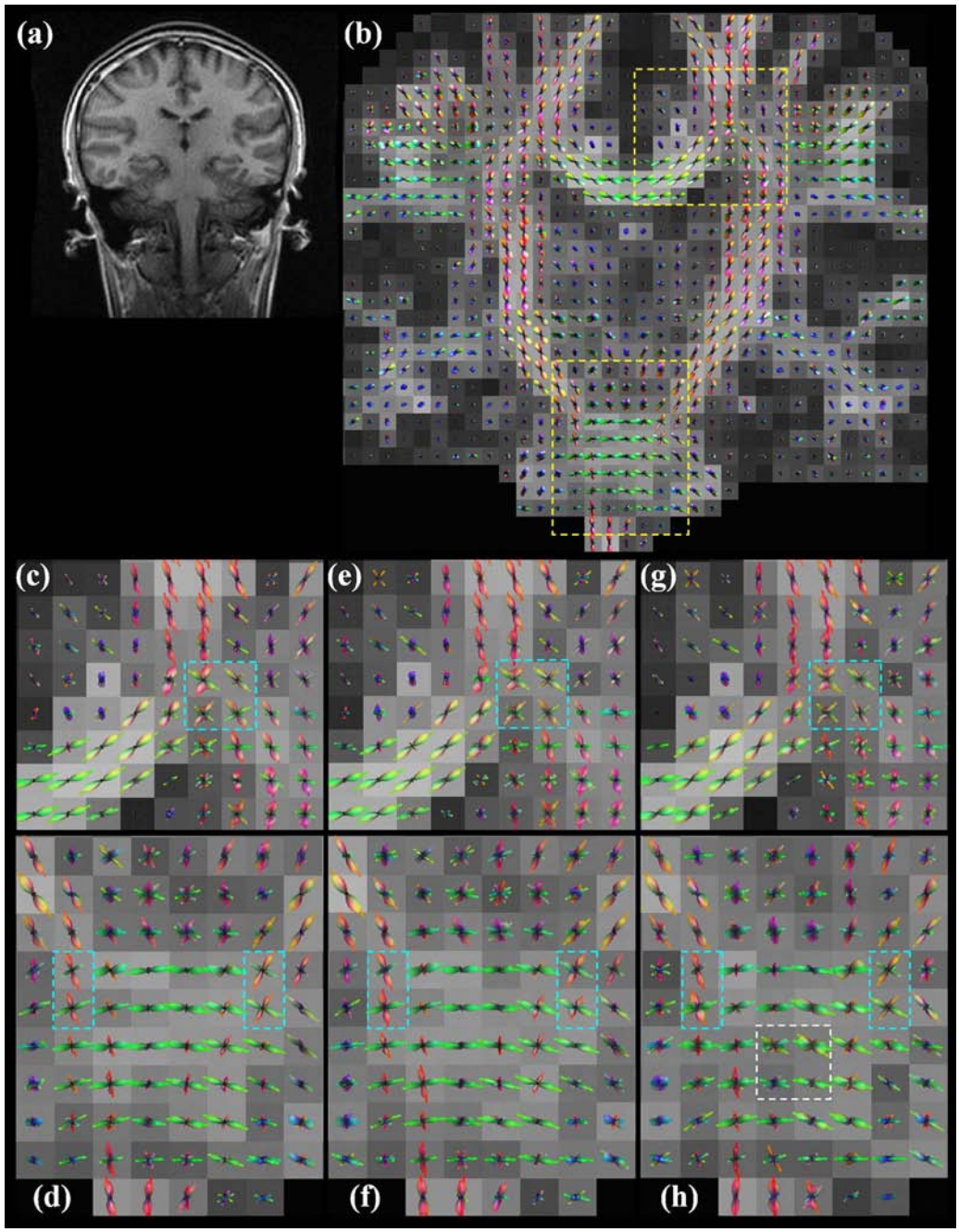

Fig. 6. Cerebral DSI and RE-DSI of a healthy human subject. (a) The corresponding brain slice on T1WI. (b) The ODF map of the complete brain slice derived from DSI-515. Zoomed ODF maps of the centrum semiovale and brainstem for (c)–(d) DSI-515, (e)–(f) RE-DSI-257, and (g)–(h) RE-DSI-123, respectively.

A. Feasibility of the Bi-Gaussian Model

In this study, we consider the bi-Gaussian model utilized in RE-DSI as a global expression of the diffusion signal attenuation function along each radial direction in q-space. The estimated signals from the bi-Gaussian are close to the experimental data, as illustrated in Fig. 1(a). Overall, RE-DSI-257 can provide better approximations to DSI-515 than RE-DSI-123. More illustrations of the bi-Gaussian fitting curves have been included in the supplementary file (Section II).

It is equivocal that the bi-Gaussian assumption in RE-DSI may fail in the presence of diffusion diffraction. Nevertheless, the diffraction pattern is unlikely to occur in practice due to the following reasons: First, in Callaghan's theory, the expression for diffusion signal that gives a diffraction pattern is formed under the assumption of a short gradient pulse [9], [35]. Meanwhile, sufficiently high q-values are required to observe the diffraction phenomenon. Both these conditions are less applicable to clinical MR scanners because of the limited gradient system. Actually, according to theory introduced by Neuman, the diffusion signal attenuation function presents a multiexponential decay curve instead of a diffraction pattern under a constant diffusion gradient waveform (i.e., $\Delta \sim \delta$) [36], which is more satisfactory to many clinical DW imaging

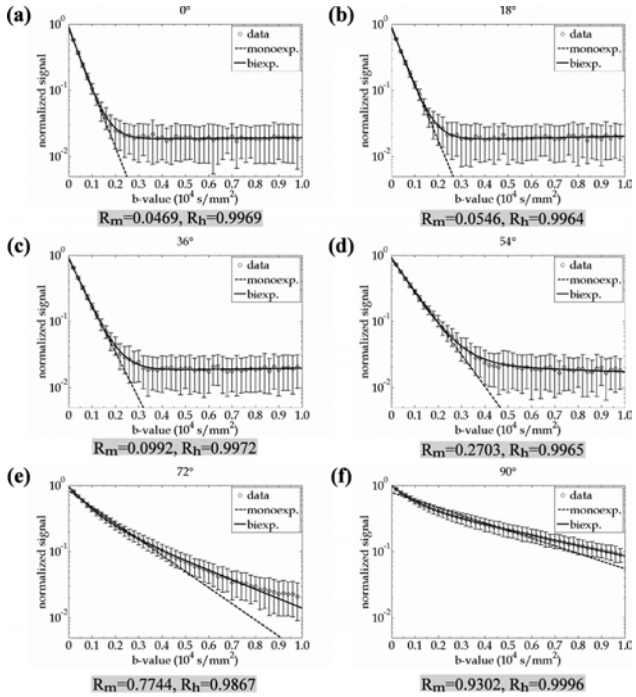

Fig. 7. (a)–(f) Signal attenuation of the experimental phantom measured at various diffusion encoding directions. The angle between the capillary tubing and gradient direction was varied from 0° to 90° with increments of 18°. Diffusion data was fitted with a mono-exponential function and a bi-exponential function, and the effectiveness of fitting was evaluated with the degrees of freedom adjusted R-square abbreviated as R_m and R_b for mono-exponential and bi-exponential fit. The signal attenuation curve was well fitted with a bi-exponential function at each gradient direction. This implied that bi-exponential diffusion signal decay was independent of the applied diffusion encoding directions.

sequences. Second, diffusion diffractions cannot be observed easily in neural tissues due to the inhomogeneity of tissue structures. Factors including axon diameter distribution, inconsistent fiber orientations, and exchange between compartments, may prohibit the occurrence of the diffraction patterns [37], [38]. Third, diffraction patterns can be observed only when the diffusion gradient direction is closely perpendicular to the fiber axis [39]. Therefore, we consider that diffusion diffraction may not vary the validity of the bi-Gaussian assumption in RE-DSI.

RE-DSI is established on the hypothesis that the diffusion signal attenuation along each radial direction in q-space can be modeled by a bi-Gaussian function. In earlier studies, the bi-exponential analyses were generally on the basis of three orthogonal diffusion directions [29], [40], [41]. Verification of the exponential attenuation assumption along each radial line in q-space has been examined through simulations [25]. It was concluded that the bi-exponential function can provide a sufficiently accurate characterization of diffusion decay curves in radial dimension since there were no significant improvements found by extension to tri-exponential function. In this study, MR data of a phantom containing coherent capillaries were further acquired to plot attenuation curves along various radial directions, as illustrated in Fig. 7. The result showed that diffusion signals fit better with a bi-exponential function than a mono-exponential function along all directions with b values ranging from 0 to 10 000 $\mathrm{s/mm^2}$. As a result, the bi-Gaussian model was suggested in q-space for RE-DSI. While it should be noted that the poor mono-exponential fit shown in Fig. 7(a) ($R_m = 0.0469$ at 0°) does not mean the non-Gaussian diffusion along the fiber axis. In practice, the diffusion decay may be deviated from a mono-exponential function due to the presence of the Rayleigh noise. Therefore, when the noise dominates the signal contribution, the bi-Gaussian kernel in RE-DSI may work as a high-pass filter and give approximations to DSI. More discussions on the relation between the noise and the bi-Gaussian curve fitting are included in the supplementary material (Section III).

B. Error Estimation of the Reduced Encoding Number

It is necessary to shorten the acquisition time as well as to meliorate the image quality in order to improve the applicability of the DSI technique in routine investigation. Half-q-DSI is a more direct approach to save the scan time in DSI since diffusion contrast is known to be positive and symmetric. While the sampling points at high q-space are required to attain sufficient angular resolution in half-q-DSI, high q-values accompanying a long TE can result in severe signal attenuation and a worse SNR of DWIs. In addition, the cross-term effect which results in unequal diffusion weightings between gradient directions may produce uncertainties in q-space analysis. On the contrary, both objectives concerning the improvement in imaging efficiency and quality can be accomplished at the same time by the simplified q-encoding schemes proposed in RE-DSI. A detailed comparison of the performance between half-q-DSI and RE-DSI is included in the supplementary material (Section I).

A reduction in the encoding number was obtained at the expense of the intrinsic angular resolution of DSI [7]. As shown in Fig. 3(b) and (c), it was evident that DSI-123 and DSI-257 were insufficient to discriminate crossing fibers at 45° due to the smoothness of the ODFs. On the contrary, RE-DSI was capable of preserving the information regarding fiber orientation while keeping the errors close to noise limit [11]. Although the UFO appeared in RE-DSI-123, as illustrated in Fig. 3(e), the peaks of the UFO were relatively smaller than that of the ODF. Thus, a threshold can be applied to filter out the contamination in order to maintain the results of fiber tracking.

C. SNR Consideration for RE-DSI

The noise influence on the bi-Gaussian kernel was assessed with a 45° crossing phantom. As expected, RE-DSI-257 demonstrated a higher resistance to noise contamination than RE-DSI-123. As shown in Table II, it was evident that the accuracy and the success rate in differentiating crossing fibers degraded due to higher noise levels. In general, parameters of the bi-Gaussian model degraded as a result of fewer q-space sampling and poor SNR for the RE-DSI. Thus, larger extrapolation errors were introduced which resulted in UFOs, consequently making primary orientations ambiguous. In practical aspects, SNRs greater than 2.5 and 3.5 in our phantom model were sufficient in allowing RE-DSI-257 and RE-DSI-123 to distinguish fibers crossing at 45°. Although SNR measurements for diffusion MR studies are usually determined with nondiffusion-weighted images, it should be noted that the ROI for measuring SNR in our phantom studies was a nonhomogeneous region containing plastic capillaries and water. Therefore, the SNR was relatively low under this condition. At the time of writing, there exists no standard

to estimate the SNR for multiple b-value diffusion studies such as DSI. A more rigorous method to define the SNR for multiple b-value diffusion studies requires further investigations.

D. RE-DSI in Biological Tissue

With manganese enhancement, specific neural fiber tracts can be distinctly identified on ME MRI. This is useful for the validation of diffusion MR techniques [5], [11]. In this study, the ME optic tract model was employed to verify RE-DSI. The results showed that the angular uncertainties in RE-DSI approached to the noise levels (See Table III), verifying that RE-DSI is applicable to the biological systems. The maps of local maximum vectors derived from RE-DSI-257 [Fig. 4(c) and Fig. 5(c)] and RE-DSI-123 [Fig. 4(d) and Fig. 5(d)] were slightly nosier than those from DSI-515 [Fig. 4(a) and Fig. 5(a)]. This is understandable since the RE-DSI was reconstructed from a decreased q-space sampling which inherently caused a reduction in the SNR [34]. Additionally, according to the phantom study on the effect of undersampling, we found that the errors would be enlarged in the bi-Gaussian curve fitting process if fewer q-space signals were sampled. In fact, this is a tradeoff between saving time and keeping a high SNR in most of the reduced-encoding techniques.

E. Limitations

Efforts have been made to analyze bi-exponential diffusion signal attenuation at high b-values using the two-tensor compartment model [28]–[31]. The inherent assumption of the model is that there is little to nearly no exchange between compartments. This may not be appropriate for the inference of diffusion compartments. Although signal decay with a b-value of up to 6000 $\mathrm{s/mm^2}$ appeared to be well-fitted with bi-exponential modeling in human brains, it was observed to be insufficient to completely describe diffusion behavior as well as to separate intracellular and extracellular compartments [30]. Additionally, previous studies demonstrated the opposite result when interpreting fast and slow diffusion associations with intracellular and extracellular space [29], [42]. In this study, the purpose of bi-Gaussian curve fitting was to model the diffusion signal decay for completeness of q-space sampling. We did not attempt to interpret the diffusion compartment with estimated parameters obtained from the bi-Gaussian kernel due to the inherent deficiency of the two-compartment model.

V. Conclusion

In this study, the RE-DSI method was proposed to facilitate the use of DSI in routine investigation. Using the reduced-encoding scheme, a noticeable reduction of the acquisition time by 50%–75% was possible while preserving the ability to resolve complex fibers. The requirement of high b-values was moderated by RE-DSI, thus allowing for the improvement of image quality with a shortened echo time. The accuracy and validity of RE-DSI was verified by the experimental phantom and ME rat models. Finally, intersections of white matter in a human brain were successfully resolved in acceptable acquisition times with RE-DSI in a clinical environment.

Acknowledgment

The authors are grateful to the National Science Council of Taiwan for support, and would like to thank V. J. Wedeen, W.-Y. Tseng, C. Chang, and J.-H. Chen for their help with the study.

References

[1] P. J. Basser, J. Mattiello, and D. LeBihan, "Estimation of the effective self-diffusion tensor from the NMR spin echo," *J. Magn. Reson. B*, vol. 103, pp. 247–54, Mar. 1994.

[2] P. J. Basser, J. Mattiello, and D. LeBihan, "MR diffusion tensor spectroscopy and imaging," *Biophys. J.*, vol. 66, pp. 259–67, Jan. 1994.

[3] P. J. Basser and C. Pierpaoli, "Microstructural and physiological features of tissues elucidated by quantitative-diffusion-tensor MRI," *J. Magn. Reson. B*, vol. 111, pp. 209–19, Jun. 1996.

[4] D. K. Jones, A. Simmons, S. C. Williams, and M. A. Horsfield, "Non-invasive assessment of axonal fiber connectivity in the human brain via diffusion tensor MRI," *Magn. Reson. Med.*, vol. 42, pp. 37–41, Jul. 1999.

[5] C. P. Lin, W. Y. Tseng, H. C. Cheng, and J. H. Chen, "Validation of diffusion tensor magnetic resonance axonal fiber imaging with registered manganese-enhanced optic tracts," *NeuroImage*, vol. 14, pp. 1035–47, Nov. 2001.

[6] M. R. Wiegell, H. B. Larsson, and V. J. Wedeen, "Fiber crossing in human brain depicted with diffusion tensor MR imaging," *Radiology*, vol. 217, pp. 897–903, Dec. 2000.

[7] V. J. Wedeen, P. Hagmann, W. Y. Tseng, T. G. Reese, and R. M. Weisskoff, "Mapping complex tissue architecture with diffusion spectrum magnetic resonance imaging," *Magn. Reson. Med.*, vol. 54, pp. 1377–86, Dec. 2005.

[8] D. G. Cory and A. N. Garroway, "Measurement of translational displacement probabilities by NMR: An indicator of compartmentation," *Magn. Reson. Med.*, vol. 14, pp. 435–44, Jun. 1990.

[9] P. T. Callaghan, *Principles of Nuclear Magnetic Resonance Microscopy*. Oxford, U.K.: Clarendon, 1991.

[10] W. S. Price, "Pulsed-field gradient nuclear magnetic resonance as a tool for studying translational diffusion. 1. Basic theory," *Concepts Magn. Reson.*, vol. 9, pp. 299–336, 1997.

[11] C. P. Lin, V. J. Wedeen, J. H. Chen, C. Yao, and W. Y. Tseng, "Validation of diffusion spectrum magnetic resonance imaging with manganese-enhanced rat optic tracts and ex vivo phantoms," *NeuroImage*, vol. 19, pp. 482–95, Jul. 2003.

[12] K. H. Cho, Y. P. Chao, Y. C. Li, J. H. Chen, and C. P. Lin, "Mapping fiber density distribution with diffusion spectrum imaging," in *Proc. 13th Annu. Meeting ISMRM*, Miami, FL, 2005, p. 577.

[13] P. Hagmann, L. Jonasson, T. Deffieux, R. Meuli, J. P. Thiran, and V. J. Wedeen, "Fibertract segmentation in position orientation space from high angular resolution diffusion MRI," *NeuroImage*, vol. 32, pp. 665–75, Aug. 2006.

[14] T. G. Reese, T. Benner, R. Wang, D. A. Feinberg, and V. J. Wedeen, "Halving imaging time of whole brain diffusion spectrum imaging (DSI) using simultaneous echo refocusing (SER) EPI," in *Proc. 14th Annu. Meeting ISMRM*, Seattle, WA, 2006, p. 1044.

[15] O. Brihuega-Moreno, F. P. Heese, C. Tejos, and L. D. Hall, "Effects of, and corrections for, cross-term interactions in q-space MRI," *Magn. Reson. Med.*, vol. 51, pp. 1048–54, May 2004.

[16] K. H. Cho, C. H. Yeh, Y. P. Chao, J. H. Chen, and C. P. Lin, "Reduce encoding of diffusion spectrum imaging with cross-term correction," in *Proc. 14th Annu. Meeting ISMRM*, Seattle, WA, 2006, p. 1043.

[17] W. Y. Chiang, V. J. Wedeen, L. Y. Kuo, M. H. Perng, and W. Y. Tseng, "Diffusion spectrum imaging using body-center-cubic sampling scheme," in *Proc. 14th Annu. Meeting ISMRM*, Seattle, WA, 2006, p. 1041.

[18] Y. C. Wu and A. L. Alexander, "Hybrid diffusion imaging," *NeuroImage*, vol. 36, pp. 617–29, Jul. 2007.

[19] L. R. Frank, "Characterization of anisotropy in high angular resolution diffusion-weighted MRI," *Magn. Reson. Med.*, vol. 47, pp. 1083–99, Jun. 2002.

[20] D. S. Tuch, T. G. Reese, M. R. Wiegell, N. Makris, J. W. Belliveau, and V. J. Wedeen, "High angular resolution diffusion imaging reveals intravoxel white matter fiber heterogeneity," *Magn. Reson. Med.*, vol. 48, pp. 577–82, Oct. 2002.

[21] D. S. Tuch, "q-ball imaging," *Magn. Reson. Med.*, vol. 52, pp. 1358–72, Dec. 2004.

[22] D. S. Tuch, T. G. Reese, M. R. Wiegell, and V. J. Wedeen, "Diffusion MRI of complex neural architecture," *Neuron*, vol. 40, pp. 885–95, Dec. 2003.

[23] K. M. Jansons and D. C. Alexander, "Persistent angular structure: New insights from diffusion magnetic resonance imaging data," *Inverse Problems*, vol. 19, pp. 1031–1046, Aug. 2003.

[24] A. W. Anderson, "Measurement of fiber orientation distributions using high angular resolution diffusion imaging," *Magn. Reson. Med.*, vol. 54, pp. 1194–206, Nov. 2005.

[25] E. Ozarslan, T. M. Shepherd, B. C. Vemuri, S. J. Blackband, and T. H. Mareci, "Resolution of complex tissue microarchitecture using the diffusion orientation transform (DOT)," *NeuroImage*, vol. 31, pp. 1086–103, Jul. 2006.

[26] K. E. Sakaie and M. J. Lowe, "An objective method for regularization of fiber orientation distributions derived from diffusion-weighted MRI," *NeuroImage*, vol. 34, pp. 169–76, Jan. 2007.

[27] J. D. Tournier, F. Calamante, D. G. Gadian, and A. Connelly, "Direct estimation of the fiber orientation density function from diffusion-weighted MRI data using spherical deconvolution," *NeuroImage*, vol. 23, pp. 1176–85, Nov. 2004.

[28] C. A. Clark and D. Le Bihan, "Water diffusion compartmentation and anisotropy at high b values in the human brain," *Magn. Reson. Med.*, vol. 44, pp. 852–9, Dec. 2000.

[29] T. Niendorf, R. M. Dijkhuizen, D. G. Norris, M. van Lookeren Campagne, and K. Nicolay, "Biexponential diffusion attenuation in various states of brain tissue: Implications for diffusion-weighted imaging," *Magn. Reson. Med.*, vol. 36, pp. 847–57, Dec. 1996.

[30] R. V. Mulkern, H. Gudbjartsson, C. F. Westin, H. P. Zengingonul, W. Gartner, C. R. Guttmann, R. L. Robertson, W. Kyriakos, R. Schwartz, D. Holtzman, F. A. Jolesz, and S. E. Maier, "Multi-component apparent diffusion coefficients in human brain," *NMR Biomed.*, vol. 12, pp. 51–62, Feb. 1999.

[31] S. E. Maier, S. Vajapeyam, H. Mamata, C. F. Westin, F. A. Jolesz, and R. V. Mulkern, "Biexponential diffusion tensor analysis of human brain diffusion data," *Magn. Reson. Med.*, vol. 51, pp. 321–30, Feb. 2004.

[32] A. Schwarcz, P. Bogner, P. Meric, J. L. Correze, Z. Berente, J. Pal, F. Gallyas, T. Doczi, B. Gillet, and J. C. Beloeil, "The existence of biexponential signal decay in magnetic resonance diffusion-weighted imaging appears to be independent of compartmentalization," *Magn. Reson. Med.*, vol. 51, pp. 278–85, Feb. 2004.

[33] M. A. Branch, T. F. Coleman, and Y. Li, "A subspace, interior, and conjugate gradient method for large-scale bound-constrained minimization problems," *SIAM J. Sci. Comput.*, vol. 21, pp. 1–23, 1999.

[34] P. J. Basser and C. Pierpaoli, "A simplified method to measure the diffusion tensor from seven MR images," *Magn. Reson. Med.*, vol. 39, pp. 928–34, Jun. 1998.

[35] P. T. Callaghan, "NMR imaging, NMR diffraction and applications of pulsed gradient spin echoes in porous media," *Magn. Reson. Imag.*, vol. 14, pp. 701–9, 1996.

[36] C. H. Neuman, "Spin echo of spins diffusing in a bounded medium," *J. Chem. Phys.*, vol. 60, pp. 4508–4511, 1974.

[37] Y. Cohen and Y. Assaf, "High b-value q-space analyzed diffusion-weighted MRS and MRI in neuronal tissues—A technical review," *NMR Biomed.*, vol. 15, pp. 516–42, Nov./Dec. 2002.

[38] S. Peled, D. G. Cory, S. A. Raymond, D. A. Kirschner, and F. A. Jolesz, "Water diffusion, T(2), and compartmentation in frog sciatic nerve," *Magn. Reson. Med.*, vol. 42, pp. 911–8, Nov. 1999.

[39] L. Avram, Y. Assaf, and Y. Cohen, "The effect of rotational angle and experimental parameters on the diffraction patterns and micro-structural information obtained from q-space diffusion NMR: Implication for diffusion in white matter fibers," *J. Magn. Reson.*, vol. 169, pp. 30–8, Jul. 2004.

[40] Y. Assaf and Y. Cohen, "Non-mono-exponential attenuation of water and N-acetyl aspartate signals due to diffusion in brain tissue," *J. Magn. Reson.*, vol. 131, pp. 69–85, Mar. 1998.

[41] D. Le Bihan, C. T. Moonen, P. C. van Zijl, J. Pekar, and D. DesPres, "Measuring random microscopic motion of water in tissues with MR imaging: A cat brain study," *J. Comput. Assist. Tomogr.*, vol. 15, pp. 19–25, Jan.-Feb. 1991.

[42] C. Nicholson and E. Sykova, "Extracellular space structure revealed by diffusion analysis," *Trends Neurosci.*, vol. 21, pp. 207–15, May 1998.